Article

Efficient Solution-Processed Photovoltaic Cells Based on an Anthradithiophene/Fullerene Blend

Matthew T. Lloyd, Alex C. Mayer, Sankar Subramanian, Devin A. Mourey, Dave J. Herman, Amit V. Bapat, John E. Anthony, and George G. Malliaras

J. Am. Chem. Soc., **2007**, 129 (29), 9144-9149• DOI: 10.1021/ja072147x • Publication Date (Web): 27 June 2007

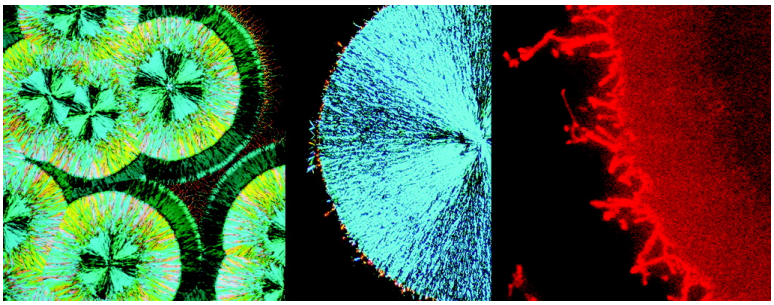

J|A|C|S
ARTICLES
Published on Web 06/27/2007

Efficient Solution-Processed Photovoltaic Cells Based on an Anthradithiophene/Fullerene Blend

Matthew T. Lloyd,[†] Alex C. Mayer,[†] Sankar Subramanian,[‡] Devin A. Mourey,[†] Dave J. Herman,[†] Amit V. Bapat,[†] John E. Anthony,[‡] and George G. Malliaras*,[†]

Contribution from the Department of Materials Science and Engineering, Cornell University, Ithaca, New York 14853, and Department of Chemistry, University of Kentucky, Lexington, Kentucky 40506

Received March 27, 2007; E-mail: ggm1@cornell.edu

Abstract: We report photovoltaic cells based on solution-processed blends using a novel anthradithiophene derivative as the donor and a fullerene derivative as the acceptor. Solvent vapor annealing of these blends leads to the formation of spherulites, which consist of a network of anthradithiophene crystallites dispersed in an amorphous matrix composed primarily of fullerene. We observe a direct correlation between coverage of a device with spherulites and its performance. Devices with 82% spherulite coverage reach a power conversion efficiency of 1%, which makes them one of the highest performing solution-processed small molecule photovoltaic cells to date.

Introduction

There has been a great deal of research on bulk heterojunction photovoltaic cells composed of polymeric donors and soluble fullerene acceptors, motivated by the facile solution processing these materials afford and by their high power conversion efficiencies, which approach 5%.[1−3] Efficient exciton dissociation within these bulk heterojunction devices depends on the formation of interpenetrating donor/acceptor networks that must be controlled at the nanometer scale.[4−6] In this regime, control of the microstructure becomes a critical factor for optimized photovoltaic response. Thus far, control of microstructure in the highest performing polymer-based photovoltaic cells is achieved by limiting the solvent evaporation rate immediately after film deposition[2] or by a postfabrication thermal annealing step.[1] These two processing steps ultimately determine the size and the composition of the donor- and acceptor-rich domains.[6,7]

In a parallel effort, organic photovoltaic cells made by vacuum-deposited small molecule heterostructures have reached power conversion efficiencies as high as 5.6%.[8] Remarkably, such efficiencies can be accomplished in multilayered device architectures where exciton generation is confined to a small volume within an exciton diffusion length of a single heterojunction. The bulk heterojunction can overcome this limitation by effectively introducing an interface within a few nanometers of all points within a device, enabling additional light absorption and extensive exciton dissociation. It is possible to combine the high charge mobility of small molecules with the increased useful volume available to bulk heterojunctions. Small molecules deposited via vacuum codeposition have been shown to yield an intimate mixture of donor and acceptor molecules.[9] Though strong photoluminescence quenching in these films suggested near 100% exciton dissociation, charge transport proved to be hindered by the lack of an optimal percolating network between the contacts. Therefore, as in the case of polymers-based bulk heterojunctions, additional processing steps are necessary to separate the donor and acceptor molecules into discrete domains where charges can find high-mobility pathways to the electrodes.[9]

Within the past few years, bulk heterojunctions utilizing solution-processable small molecules as the donor and the acceptor have made their debut.[10−13] Soluble small molecules are attractive for photovoltaic cells as they offer the facile processing associated with polymers, yet are easier to synthesize and purify, are monodisperse, and show, in general, higher mobilities.[14] Table 1 summarizes efforts to employ small molecules for solution-processed organic photovoltaic cells. The

[†] Cornell University.
[‡] University of Kentucky.

(1) Ma, W.; Yang, C.; Gong, X.; Lee, K.; Heeger, A. J. *Adv. Funct. Mater.* **2005**, *15*, 1617.
(2) Li, G.; Shrotriya, V.; Huang, J. S.; Yao, Y.; Moriarty, T.; Emery, K.; Yang, Y. *Nat. Mater.* **2005**, *4*, 864.
(3) Kim, Y.; Cook, S.; Tuladhar, S. M.; Choulis, S. A.; Nelson, J.; Durrant, J. R.; Bradley, D. D. C.; Giles, M.; Mcculloch, I.; Ha, C. S.; Ree, M. *Nat. Mater.* **2006**, *5*, 197.
(4) Halls, J. J. M.; Walsh, C. A.; Greenham, N. C.; Marseglia, E. A.; Friend, R. H.; Moratti, S. C.; Holmes, A. B. *Nature* **1995**, *376*, 498.
(5) Yu, G.; Gao, J.; Hummelen, J. C.; Wudl, F.; Heeger, A. J. *Science* **1995**, *270*, 1789.
(6) Hoppe, H.; Sariciftci, N. S. *J. Mater. Chem.* **2006**, *16*, 45.
(7) McNeill, C. R.; Watts, B.; Thomsen, L.; Belcher, W. J.; Kilcoyne, A. L. D.; Greenham, N. C.; Dastoor, P. C. *Small* **2006**, *2*, 1432.
(8) Chan, M. Y.; Lai, S. L.; Fung, M. K.; Lee, C. S.; Lee, S. T. *Appl. Phys. Lett.* **2007**, *90*, 023504.
(9) Peumans, P.; Uchida, S.; Forrest, S. R. *Nature* **2003**, *425*, 158.
(10) Schmidt-Mende, L.; Fechtenkotter, A.; Mullen, K.; Moons, E.; Friend, R. H.; MacKenzie, J. D. *Science* **2001**, *293*, 1119.
(11) Roncali, J.; Frere, P.; Blanchard, P.; de Bettignies, R.; Turbiez, M.; Roquet, S.; Leriche, P.; Nicolas, Y. *Thin Solid Films* **2006**, *511*, 567.
(12) Sun, X. B.; Zhou, Y. H.; Wu, W. C.; Liu, Y. Q.; Tian, W. J.; Yu, G.; Qiu, W. F.; Chen, S. Y.; Zhu, D. B. *J. Phys. Chem. B* **2006**, *110*, 7702.
(13) Roquet, S.; Cravino, A.; Leriche, P.; Aleveque, O.; Frere, P.; Roncali, J. *J. Am. Chem. Soc.* **2006**, *128*, 3459.
(14) Hulea, I. N.; Fratini, S.; Xie, H.; Mulder, C. L.; Iossad, N. N.; Rastelli, G.; Ciuchi, S.; Morpurgo, A. F. *Nat. Mater.* **2006**, *5*, 982.

10.1021/ja072147x CCC: $37.00

Table 1. Comparison of Solution-Processed Small Molecule Photovoltaic Cells[a]

materials system	J_{sc} (mA/cm^2)	V_{oc} (mV)	FF	I (mW/cm^2)	η_P (%)	D/A	ref
ITO/hexaphenyl-substituted hexabenzocoronene:*N*,*N*′-bis (1-thylpropyl)-3,4,9,10-perylenebis (dicarboximide) (perylene)/Al	0.034	690	0.40	0.47	*b*	60:40	Schmidt-Mende et al. (10)
ITO/PEDTO:PSS/star-shaped oligothiophene:PCBM/CsF/Al	1.15	850	0.24	80	0.3%	37:63	Roncali et al. (11)
ITO/PEDOT:PSS/X-shaped oligothiophene:PCBM/Al	3.65	850	0.26	100	0.8%	45:55	Sun et al. (12)
ITO/PEDOT:PSS/star-shaped triphenylamine:PCBM/Al	4.10	660	0.30	100	0.8%	25:75	Roquet et al. (13)
ITO/PEDOT:PSS/ethyl-TES-ADT:PCBM/CsF/Al	2.96	840	0.40	100	1%	70:30	this work

[a] J_{sc} is the short-circuit current density, V_{oc} is the open-circuit voltage, FF is the fill factor, I is incident light intensity, η_P is power conversion efficiency, and D/A is the donor/acceptor blending ratio by weight. [b] Peak external quantum efficiency of 34% reported for low light intensity.

Scheme 1. Synthesis of Ethyl-TES-ADT

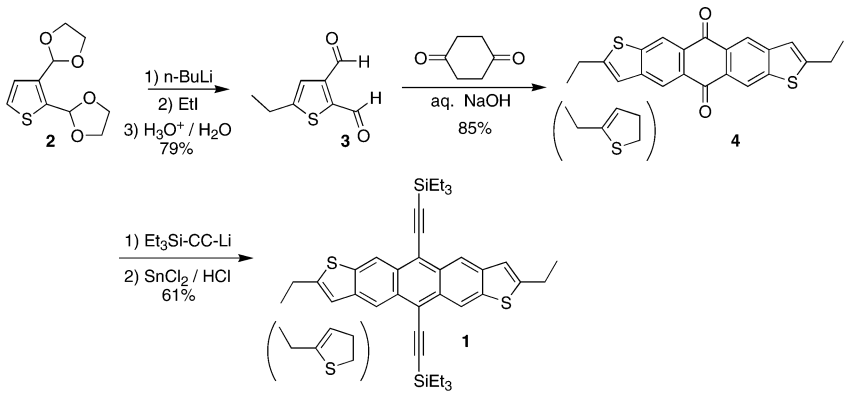

Cambridge group first exploited the capability of semiconducting liquid crystals to form continuous spin-cast films with stratified microstructures.[10] Hexabenzocoronene self-organizes into discotic, vertically segregated columns which can be infiltrated with a perylene-derived electron acceptor. Photodiodes fabricated from these materials displayed impressive external quantum efficiencies (up to 34%); however, illumination intensity greater than $^1/_{100}$ of one sun resulted in rapid photoinduced degradation. Others have measured promising performance for branched oligothiophenes[11,12] and triphenylamine derivatives[13] in blends with soluble fullerene acceptors. These efforts, which have led to power conversion efficiencies up to 0.8%, have thus far focused on synthesis of new compounds and proof-of-concept. The influence of processing conditions on the evolution of morphology and crystallinity has received little attention.

In this article, we report photovoltaic cells using solution-processed donor/acceptor blends that show a power conversion efficiency of 1%. A novel anthradithiophene derivative, 2,8-diethyl-5,11-bis(triethylsilylethynyl)anthradithiophene (ethyl-TES-ADT—structure shown in Scheme 1), was used as the donor, a choice motivated by the fact that acene derivatives have high solubility in common solvents and excellent charge charier mobility.[15−17] As an acceptor we used the C_{60} derivative (6,6)-phenyl C_{61} butyric acid methyl ester (PCBM), a standard choice for solution-processed photovoltaic cells. The high performance of this blend was found to be a result of crystallization in an unusual spherulite motif, induced by solvent vapor annealing. The structure of the spherulites was analyzed with optical microscopy, atomic force microscopy (AFM), and X-ray diffraction and found to consist of a network of anthradithiophene crystallites dispersed in an amorphous matrix composed primarily of fullerene. These results demonstrate that high efficiency can be achieved by control of microstructure in solution-processed small molecule blends.

Experimental Section

Materials. Triethylsilyl acetylene was used as purchased from GFS Chemicals. Tetrahydrofuran (THF) was distilled over sodium prior to use, while all other solvents were used without further purification. Poly(3,4-ethylene dioxythiophene):poly(styrenesulfonate) (PEDOT:PSS) was purchased from Baytron, and PCBM was purchased from NanoC. Other reagents were purchased from Aldrich or synthesized by literature procedures. Column chromatography was performed with silica gel (60 Å, 32−63 μm) from Sorbent Technologies.

5-Ethyl Thiophene-2,3-dicarboxaldehyde (3). To a solution of diacetal **2**[18] (21 mmol) dissolved in THF (60 mL) in a flame-dried round-bottom flask cooled to −78 °C under a dry nitrogen atmosphere was added slowly 27.4 mmol of *n*-BuLi (hexane solution). After 1 h, ethyl iodide (29.5 mmol) was added, and the reaction mixture was warmed to room temperature and stirred overnight. The reaction mixture was quenched by adding cold water very carefully, extracted with diethyl ether, and washed with water. The organic layer was dried with anhydrous $MgSO_4$ and concentrated. The acetal groups were hydrolyzed by stirring the material vigorously in a 3 M HCl/THF (1/1) solution for 1 h. The resulting product was purified by column chromatography using hexanes/dichloromethane (120 mL/180 mL). Yield = 79%. ^{1}H NMR (200 MHz, $CDCl_3$): δ 1.37 (t, J = 3.75 Hz, 3H), 2.92 (q, J = 3.8 Hz, 2H), 7.34 (s, 1H), 10.33 (s, 1H), 10.39 (s, 1H) ppm. ^{13}C NMR (50 MHz, $CDCl_3$): δ 14.99, 23.71, 126.24, 143.98, 144.80, 157.59, 182.20, 184.85 ppm. MS (EI 70 eV): m/z 168 (M^+), 140 (M^+ − CHO).

2,8-Diethyl Anthradithiophenequinone (4) (Mixture of syn and anti Isomers). A few drops of 15% aqueous KOH solution were added to a mixture of 1.4-cyclohexanedione (0.6 g, 5.5 mmol) and 5-ethyl

(15) Anthony, J. E.; Brooks, J. S.; Eaton, D. L.; Parkin, S. R. *J. Am. Chem. Soc.* **2001**, *123*, 9482.
(16) Dickey, C. D.; Anthony, J. E.; Loo, Y.-L. *Adv. Mater.* **2005**, *18*, 1721.
(17) Park, S. K.; Kuo, C. C.; Anthony, J. E.; Jackson, T. N. *2005 International Electron Device Meeting Technical Digest*; 2006; p 113.
(18) Laquindanum, J. G.; Katz, H. E.; Lovinger, A. J. *J. Am. Chem. Soc.* **1998**, *120*, 664.

thiophene dialdehyde **3** (1.8 g, 11.0 mmol) dissolved in THF/ethanol (5 mL/15 mL) in a 100 mL round-bottom flask, and the mixture was stirred at room temperature for 3 h. The yellow precipitate was filtered, washed with ether, and dried in air to yield 85% of desired (insoluble) quinone. MS (MALDI, TCNQ matrix): m/z 377 (100%, $M^+ + 1$).

2,8-Diethyl-5,11-bis(triethylsilylethynyl)anthradithiophene (1). *n*-BuLi (1.86 mL, 4.66 mmol) was added to triethylsilyl acetylene (0.95 mL, 5.32 mmol) dissolved in hexanes (50 mL) under N_2 at room temperature in a dried 500 mL round-bottom flask. This mixture was stirred for 30 min, after which time quinone **4** (0.5 g, 1.33 mmol) and additional hexanes (200 mL) were added. The resulting suspension was stirred and heated at 66 °C for 12 h, after which time stannous chloride (0.9 g, 3.99 mmol), 0.5 mL of water, and 1.5 mL of 10% aqueous H_2SO_4 were added, and the reaction mixture was heated for 5 h. After this mixture was cooled and dried over anhydrous $MgSO_4$, it was immediately flushed through a silica gel plug and eluted with hexanes. The mixture was evaporated to dryness, and the product further purified by crystallization from hexanes to yield 61% of pure product, mp: 215 °C. ^{1}H NMR (200 MHz, $CDCl_3$): δ 0.92 (q, $J = 3.9$ Hz, 12H), 1.26 (t, $J = 3.85$ Hz, 18H), 1.46 (t, $J = 3.75$ Hz, 6H), 3.00 (q, $J = 3.73$ Hz, 4H), 7.12 (s, 2H), 8.92 (s, 2H), 9.03 (s, 2H) ppm. ^{13}C NMR (50 MHz, $CDCl_3$): δ 4.91, 7.91, 14.90, 24.94, 103.96, 106.18, 117.26, 119.39, 119.53, 119.62, 119.86, 119.95, 129.70, 130.19, 140.05, 141.22, 151.84, 151.89 ppm. MS (70 eV, EI): m/z 622 (25%, $M^+ - 1$), 623 (15%, M^+). Anal. Calcd (%): C, 73.25; H, 7.44. Found (%): C, 73.21; H, 7.51.

Measurements. ^{1}H and ^{13}C NMR spectra were recorded on Varian (Gemini 200 MHz/Unity 400 MHz) spectrometers with tetramethyl silane as the internal standard. Mass spectral analyses were performed in EI mode on a JEOL (JMS-700T) mass spectrometer or in MALDI mode on a Bruker Daltonics Autoflex. Electronic spectral analyses were performed on a Shimadzu UV-2501. Electrochemical data were collected on a BAS CV-50W voltammetric analyzer, performed in 0.1 M Bu_4NPF_6 in dichloromethane, with ferrocene as an internal standard. Single-crystal X-ray analyses were performed on a Nonius kappaCCD machine with a sealed-tube molybdenum X-ray source.

Device Fabrication and Characterization. PEDOT:PSS was spin cast to form a thin film (60 nm) on prepatterned indium−tin oxide (ITO)-coated glass slides. Individual 40 mg/mL solutions of ethyl-TES-ADT and PCBM in toluene and *o*-dichlorobenzene, respectively, were blended to give a ethyl-TES-ADT:PCBM weight ratio of 70:30. This composition consistently delivered the highest power conversion efficiency. Solutions were allowed to stir for 10 min at room temperature before spin coating at 1000 rpm for 1 min in ambient. The films were solvent vapor annealed as described below, and cathodes consisting of a 10 Å layer of CsF followed by 400 Å of Al were thermally deposited under vacuum ($\sim 10^{-6}$ torr). The devices were tested in a nitrogen environment using a halogen lamp (Solex) with an illumination intensity of 100 mW/cm^2. The light intensity was measured with a calibrated UV-enhanced silicon photodiode (Edmund Optics) and, to check for consistency, a UDT S370 optometer coupled to an integrating sphere. AFM images were captured with a Digital Instruments DI3000 in tapping mode. An Olympus BH-2 fluorescence microscope with a filter cube attachment and xenon light source was used to image spherulite growth. Polarized light microscopy was performed on an Olympus BX51. X-ray diffraction scans were collected with a Scintag diffractometer in both $\theta-2\theta$ and rocking modes.

Results and Discussion

Ethyl-TES-ADT (**1**) was synthesized (Scheme 1) as an inseparable mixture of syn and anti isomers in good overall yield. The material precipitated readily from hexanes, yielding red, block-shaped crystals. X-ray analysis showed the aromatic chromophores adopt a one-dimensional π-stacked arrangement (Figure 1), with excellent π-overlap and $C_{Ar}-C_{Ar}$ contacts as close as 3.47 Å. Solutions of ethyl-TES-ADT mixed with PCBM showed no reaction between these materials over a period of several months. This is in marked contrast with the carbocyclic acenes, which undergo Diels−Alder reaction with fullerene and fullerene derivatives rapidly in solution.[19]

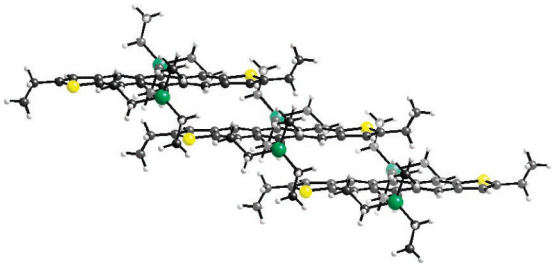

Figure 1. Crystal packing of ethyl-TES-ADT, showing the 1-D π-stacking motif.

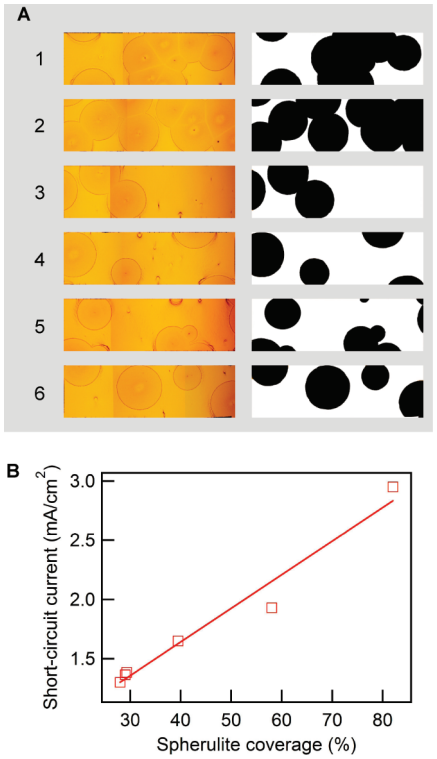

Figure 2. (A) Optical micrographs from six devices and the corresponding digital images used to calculate spherulite coverage. Each micrograph shown corresponds to the entire device area of 3 × 1 mm^2. (B) Short-circuit current as a function of spherulite coverage for these six devices. The line is a linear fit to the data ($r^2 = 0.98$).

The stability of ethyl-TES-ADT:PCBM solutions allows for deposition of these films by spin coating in air. Optical fluorescence microscopy indicated complete photoluminescence quenching of the otherwise highly fluorescent ethyl-TES-ADT, while cross-polarized microscopy pointed to an absence of crystal formation. X-ray diffraction scans of the as-cast films were also featureless. When blends of ethyl-TES-ADT:PCBM were exposed to solvent vapor, crystallization occurred as manifested by the appearance of spherulites (Figure 2A). While a variety of solvents were found to induce crystallization, the best photovoltaic performance was obtained by transferring the films immediately after spin coating into a 1 in. fluoroware sample holder and sealing it tight. Sufficient residual solvent

(19) Miller, G. P.; Mack, J. *Org. Lett.* **2000**, *2*, 3979.

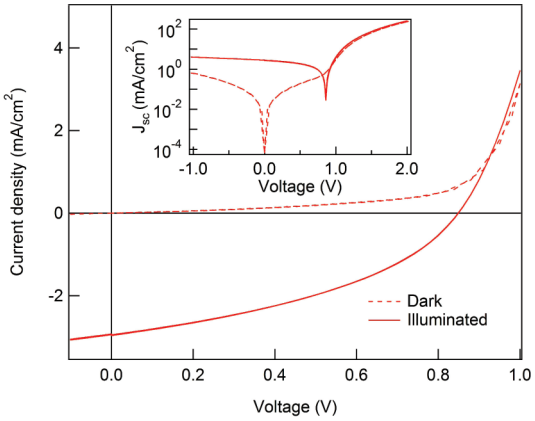

Figure 3. Current−voltage characteristics of a device with 82% spherulite coverage, in the dark (dashed) and under illumination with 100 mW/cm^2 (solid).

was contained within the spin-coated films to induce vapor annealing and lead to the formation of spherulites. The latter grew as large as 1 mm in diameter and covered a large area of the film.

The presence of spherulites was found to have a profound effect on device performance. Figure 2A shows optical micrographs of six devices, all on the same wafer, taken through the transparent ITO electrode. The variation in spherulite coverage is a result of the low nucleation density of the spherulites and its random character. For clarity, these micrographs were digitally processed to illustrate areas covered with spherulites as black on a white background. The short-circuit current measured in these devices is shown in Figure 2B to be proportional to spherulite coverage. At the same time, neither the open-circuit voltage nor the fill factor changed appreciably with spherulite coverage. Therefore, the device efficiency was found to increase with the fraction of device area covered with spherulites.

Figure 3 shows the current−voltage characteristics for the best device, which corresponds to 82% spherulite coverage. A short-circuit current density of 2.96 mA/cm^2, an open-circuit voltage of 840 mV, and a fill factor of 0.40 result in a power conversion efficiency of 1%. It should be noted that the open-circuit voltage is consistent with the difference between the HOMO of ethyl-TES-ADT (5.15 eV) and the LUMO of PCBM (3.9 eV) including a ∼0.2 eV loss at each electrode, as expected.[20]

Small molecule films are known to restructure upon exposure to a solvent vapor.[16,21] Gregg subjected vacuum-deposited films of perylene bis(phenethylimide) to methylene chloride vapor.[21] Upon exposure to the vapor the films became increasingly crystalline over the course of several hours. Solvent vapor annealed photovoltaic devices showed an estimated 76% enhancement in exciton diffusion length and a 10-fold increase in photocurrent. In another study, Dickey et al. exposed a film of soluble anthradithiophene to an environment saturated with dichloroethane vapor.[16] This produced exceptionally large (>1 mm^2) single-crystal domains. In terms of device performance, solvent vapor anneal increased hole mobility by nearly 2 orders of magnitude, up to 0.11 cm^2/V•s. Both effects (increase in exciton diffusion length and charge carrier mobility) associated with crystallization are beneficial to photovoltaic performance and can help understand the trend observed in Figure 2B.

Spherulites are often seen in polymeric systems when supercooled from the melt or processed from moderately saturated solutions.[22,23] In this case, the spherulites are comprised of multiarmed crystalline filaments of tightly kinked polymer chains radially aligned in spherical domains. When imaged through crossed polarizers, such spherulites are easily identifiable by a Maltese cross signature, which reflects their radial alignment. Spherulites also tend to form in thin films of liquid crystals[24] and are occasionally noted in solid films of small molecules,[25] where they arise from radially oriented needle-shaped crystals that emerge from a common center.[26]

In order to understand the structure of the spherulites in ethyl-TES-ADT:PCBM blends, their evolution was followed using polarized and fluorescence microscopy. For these experiments, films were solvent vapor annealed as described above for a given amount of time (1, 2, and 3 min) and then heated to 80 °C to remove excess solvent and freeze-in the obtained microstructure. As shown in Figure 4A, the spherulites evolve by nucleation and radial growth of needle-shaped crystallites, consistent with the appearance of the Maltese cross.

Information regarding the composition of the spherulites can be obtained from the fluorescence images (Figure 4B), which selectively monitor ethyl-TES-ADT due to its high fluorescence quantum yield. These images reveal complete quenching of ethyl-TES-ADT outside of the spherulites, indicating rather intimate mixing of the donor and acceptor molecules. On the other hand, the spherulites are shown to be rich in ethyl-TES-ADT. The fluorescence spectrum of the spherulites (not shown here) is the same as that of pure ethyl-TES-ADT films.

Atomic force microscopy images (Figure 4C) corroborate the presence of an amorphous blend outside the spherulites. They also show that the spherulites consist of elongated crystallites that are of the order of a micrometer long and 100 nm wide, considerably smaller than the needle-like crystals seen in the optical micrographs. No obvious correlation in the orientation of these crystallites is evident in this figure. However, the amount of orientation that is needed to affect light polarization is very small and not necessarily discernible in an AFM image. It should be mentioned that the crystallites close to the edge of the spherulite were considerably larger that those at the interior, a finding that can explain the appearance of a ring (Figure 4, parts A and B) at the periphery of the spherulites.

X-ray diffraction (Figure 5) from a thin film with a high spherulite coverage shows Bragg peaks that correspond to a lattice spacing of 10.27 Å, demonstrating that the spherulites are composed of crystals of ethyl-TES-ADT.[27] These same X-ray diffractions scans do *not* reveal evidence of crystalline regions of PCBM crystals.[28] The exclusive presence of (0*k*0) reflections from ethyl-TES-ADT indicates that the crystallites

(20) Mihailetchi, V. D.; Blom, P. W. M.; Hummelen, J. C.; Rispens, M. T. *J. Appl. Phys.* **2003**, *15*, 6849.
(21) Gregg, B. A. *J. Phys. Chem.* **1996**, *100*, 852.
(22) Magill, J. H. *J. Mater. Sci.* **2001**, *36*, 3143.
(23) Granasy, L.; Pusztai, T.; Tegze, G.; Warren, J. A.; Douglas, J. F. *Phys. Rev. E* **2005**, *72*, 011605.
(24) Rinne, F. *Trans. Faraday Soc.* **1933**, *29*, 1016.
(25) Yu, L. *Cryst. Growth Des.* **2003**, *3*, 967.
(26) Magill, J. H.; Plazek, D. J. *J. Chem. Phys.* **1967**, *46*, 3757.
(27) Single-crystal measurements indicate unit cell dimensions as follows: a = 7.9028(3) Å, b = 10.44873(4) Å, c = 10.8412(5) Å, with angles α = 76.3218(18)°, β = 88.4391(17)°, and γ = 88.9630(19)°.
(28) Erb, T.; Zhokhavets, U.; Gobsch, G.; Raleva, S.; Stuhn, B.; Schilinsky, P.; Waldauf, C.; Brabec, C. J. *Adv. Funct. Mater.* **2005**, *15*, 1193.

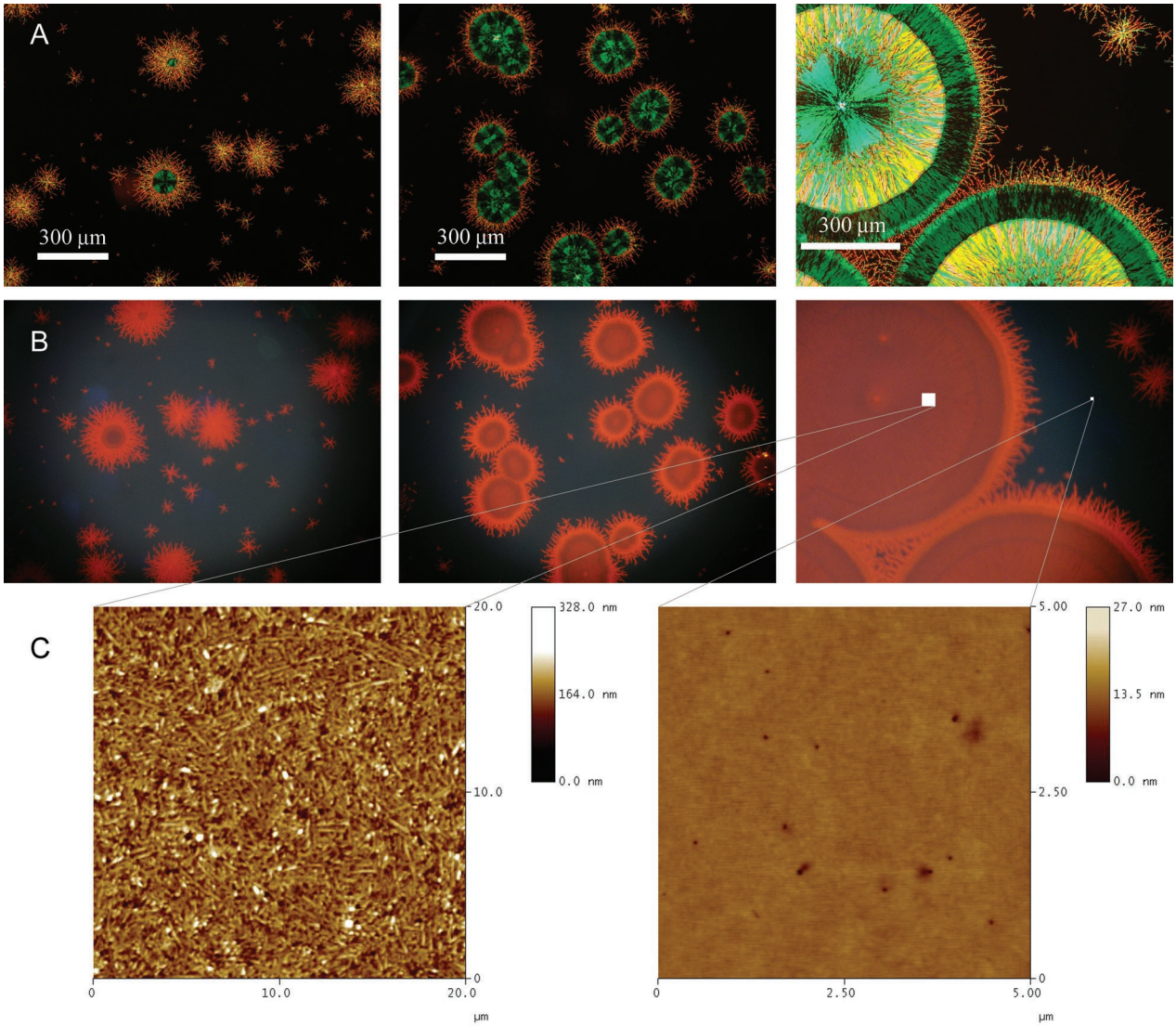

Figure 4. Optical micrographs of spherulite growth as seen through crossed polarizers (A) and by fluorescence (B). Spherulite growth induced by annealing with residual solvent vapor after 1 min (first column), 2 min (second column), and 3 min (third column). (C) AFM images inside and outside of a spherulite.

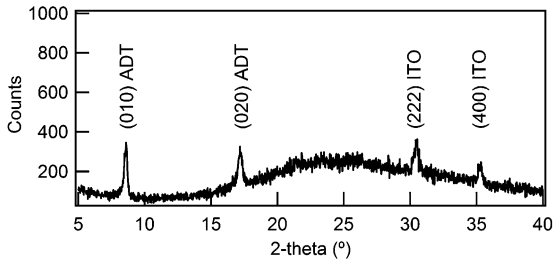

Figure 5. X-ray diffraction pattern for a film with a high degree of spherulite coverage showing reflections that correspond to crystals of ethyl-TES-ADT and the ITO substrate.

are oriented predominantly with their *b*-axis perpendicular to the substrate. However, rocking scans about the (010) peak (not shown here) revealed considerable orientational disorder along the direction perpendicular to the substrate.

According to the above, the following picture emerges regarding spherulite growth in ethyl-TES-ADT:PCBM blends: Once a stable nucleus forms, ethyl-TES-ADT aggregates into crystals which exclude PCBM. The latter occupies the space between these crystals and remains inside the spherulites. The nucleation of ethyl-TES-ADT is random, and we did not attempt to control it. These crystals grow unimpeded in the direction away from the nucleus, while growth along a tangential direction is limited by collisions with neighboring crystals. The result is an advancing front, composed of radially oriented needle-like crystals, as seen by optical microscopy. The smaller crystallites (micrometer long, 100 nm wide) observed with AFM (Figure 4C) in the interior of the spherulites are likely a result of a breakup of these needles, an effect that could be caused by a Rayleigh instability.[29] As a result of this breakup, the orientation of the crystallites is randomized to the extent that it does not show macroscopic orientation in an AFM image but still maintains enough orientation to affect light polarization.

The solvent vapor annealing process described here yielded devices with a maximum spherulite coverage of 82%. Assuming that one could optimize this process to obtain 100% coverage, and given that efficiency is proportional to spherulite coverage, a maximum efficiency of 1.2% could be achieved. A useful benchmark for the ultimate efficiency of photovoltaic cells based

(29) Reiter, G. *Langmuir* **1993**, *9*, 1344.

on ethyl-TES-ADT:PCBM blends can be obtain from the calculation of Scharber et al.[30] On the basis of the HOMO (5.15 eV) and LUMO (2.98 eV) levels of ethyl-TES-ADT (measured in solution by cyclic voltammetry), and assuming an external quantum efficiency of 65% and a fill factor of 0.65, the power conversion efficiency benchmark is 2.5%. One reason for being below this mark is that the ethyl-TES-ADT crystallites within the spherulites are too large to achieve efficient quenching of excitons, as evidenced by the fluorescence emission from the spherulites. Optimization of the thickness of the blend, as well as control of the dimensions of the crystallites within the spherulites, should lead to devices that perform closer to that limit. For the latter, we found that exposure to different solvent vapors led to a variation of the size of the spherulites and the size of the ethyl-TES-ADT crystallites within these. A better understanding and control of this process is needed.

Ultimately, a higher efficiency can be achieved by designing donor molecules with a smaller band gap to improve long-wavelength absorption. At the same time, the HOMO and LUMO levels of these molecules should be carefully engineered to maximize open-circuit voltage. The calculation of Scharber et al.[30] predicts an efficiency of 10% for donor/acceptor blends utilizing a fullerene acceptor. Therefore, there is much room for improvement. Acenes are amenable to facile energy level tuning, and screening efforts are currently underway for small band gap and appropriate energy levels.

In summary, we demonstrated high-efficiency photovoltaic cells from a novel anthradithiophene-based donor. The high solubility of this molecule to common organic solvents and the absence of reactions with fullerene acceptors enables the facile fabrication of photovoltaic devices. Solvent vapor annealing causes a reorganization of the donor/acceptor blends into spherulites comprised of ethyl-TES-ADT crystallites. Their photovoltaic performance was found to be directly dependent on spherulite coverage, leading to devices with a power conversion efficiency of 1%.

Acknowledgment. This work was made possible by funding from the Office of Naval Research. Additional thanks are due to the Cornell Center of Materials Research, and the Nanobiotechnology Center, as well as John Hunt, Carol Bayles, and Maura Weathers for assistance with characterization of the films.

Supporting Information Available: Supplementary Figure 1. This material is available free of charge via the Internet at http://pubs.acs.org.

JA072147X

(30) Scharber, M. C.; Wuhlbacher, D.; Koppe, M.; Denk, P.; Waldauf, C.; Heeger, A. J.; Brabec, C. L. *Adv. Mater.* **2006**, *18*, 789.